Phase transformation of iron under shock compression: Effects of voids and shear stress

Xinlin Cui,[1,2] Wenjun Zhu,[1] Hongliang He,[1,*] Xiaoliang Deng,[1] and Yingjun Li[2]
[1]*Laboratory for Shock Wave and Detonation Physics Research, Institute of Fluid Physics, P.O. Box 919-102, Mianyang 621900, People's Republic of China*
[2]*School of Mechanics and Civil Engineering, China University of Mining and Technology (Beijing), Beijing 100083, People's Republic of China*
(Received 14 August 2007; revised manuscript received 16 June 2008; published 22 July 2008)

Unlike the perfect single crystals, most engineering materials contain a large number of defects that would affect their properties critically. By introducing a nanovoid into the single-crystal iron, the shock-induced phase transformation of body-centered cubic α phase to hexagonal close-packed ε phase has been investigated by means of molecular-dynamics (MD) simulation. Results have revealed that the threshold pressure and the nucleation velocity of $\alpha \rightarrow \varepsilon$ phase transformation are significantly different from that of the perfect single-crystal iron. The nanovoid has reduced the threshold pressure and accelerated the nucleation speed, which induces the new phase to generate and grow much easier. The effects of the void size on the phase transformation are also illustrated. Furthermore, the nanovoid also has affected the phase transformation district. In the case of perfect single-crystal iron, the homogeneous transformation is observed beginning from the leading front of the shock wave, but in the defective crystal iron it first occurs around the edge of the nanovoid, and then forms a butterfly-shaped phase transformation zone due to the slippage of the atoms in the (011) and $(01-1)$ planes along the $[01-1]$ and $[011]$ directions on the surface of the void. The effect of shear stress on the phase transformation of iron has been analyzed in detail as well. By calculating the distribution of the resolved shear stress along the slip plane of the shocked crystal iron, the relationship between the shear stress and the slip plane has been discussed.

DOI: 10.1103/PhysRevB.78.024115 PACS number(s): 61.50.Ks, 68.35.Rh, 91.60.Ed, 31.15.xv

I. INTRODUCTION

Phase transformation of iron under high pressure and high temperature is of great interest in condensed-matter physics, materials science, and geophysics.[1–3] The solid to solid phase transformation of $\alpha \rightarrow \varepsilon$ in iron was first reported by Bancroft *et al.*[4] in 1956 under the shock wave compression with the measurement of Hugoniot equation of state (EOS). The shock pressure of this transformation was determined as about 13 GPa. Following this observation, many studies have been focused to discuss the properties of $\alpha \rightarrow \varepsilon$ phase transformation both in theory and at experiment (static high pressure and shock wave compression).[5–9] The micromechanism of this transformation has been previously suggested,[10] and recently confirmed with the MD simulations.[11–13] Given the details of tracking the transformation, the MD simulation may provide a new understanding in physics for the solid-solid phase transformation under the shock wave compression, which is poorly understood due to its rapid alteration in the experimental measurement.

In engineering application, most materials contain large number of defect concentrations, such as void, grain boundary, dislocation, etc. These defects may affect the phase transformation property of material, and so does iron. Knowledge about the defect's influence on the phase transformation of iron is necessary for a physical understanding of shock wave compression. In addition, the effect of the shear stress on the phase transformation of iron has been confirmed,[14] but the detail explanation in microstructure has not been completed, although a few theoretical studies have pursued.[14,15] The shear stress is also important in the case of shock wave compression, because a large shear stress would be produced in the shock compressed material due to the strong lateral confinement of the uniaxial strain.

By means of MD simulation, this work is to present the microview as well as the wave profile analyses on the phase transformation of iron with a nanovoid and to understand the role of defect under shock compression. Our results indicate that the nanovoid is the favorite nucleation site of the phase transformation of iron and it accelerates the transformed phase district expansion, also it decreases the pressure threshold of the phase transformation. Due to the slippage of the atoms around the edge of the nanovoid along $[01-1]$ and $[011]$ directions, the hcp structure initiates from four symmetric locations on the surface of the void and yields a butterfly-shaped transformation pattern. The obvious difference has been further confirmed by the particle velocity profiles. The existence of the nanovoid induces "inhomogeneity spot" (or "hot spot") and changes the macroscopic response, such as lower particle velocity in the defective iron. The void size also affects the threshold pressure and the nucleation speed. Furthermore, based on the distribution of the resolved shear stress along the slip plane of the shocked iron, we discussed the relationship between the shear stress and the slip plane during the transformation.

II. MOLECULAR-DYNAMICS SIMULATION

The scheme of our MD simulation previously has been used to study the lattice orientation effect on the nanovoid growth in copper under shock loading, and the details can be found elsewhere.[16] For this work, the potential function adopted is the embedded atom method (EAM) potential[17,18] proposed by Harrison *et al.*,[19] which has successfully de-

scribed the phase transformation in iron under dynamic and static conditions. The molecular-dynamics simulation of up to about 2.0×10^6 atoms was used to ensure that our simulations were larger enough to cover both the atomistic details and the phase transformation microstructure. The simulated sample was $45.9\times22.9\times22.9$ nm in size. In order to illustrate the effect of the void on the phase transformation, two kinds of the samples were used. One kind of sample was a settled nanovoid of 1.0 nm in diameter in the single-crystal iron, formed by removing 59 atoms from the sample, and the center of the void is 17.2 nm (60 lattice constant) far away from the impact face, and the other kind of sample was a perfect single-crystal iron. The shock wave compression was generated using the momentum mirror method[20] along [100] direction. To minimize the surface and edge effects, the periodic boundary conditions were applied in the lateral directions. The end of the sample farthest from the piston was settled as a free surface. Different compression pressures in the sample were generated by changing the velocity of the piston. The trajectory of each atom was integrated by a predict-correct scheme at a time step of 1 fs. Because of the shock compression, the system could be taken as adiabatic, and the initial temperature was assumed as 0 K.

III. RESULTS AND DISCUSSION

For describing the characters of the structure phase transformation and checking the course of the phase transformation, "the pair analyze"[21] technology has been used to distinguish the different structure phases. When the shock compression pressure reaches the critical pressure, new structure atoms nucleate in the shock compressed crystal, and above the pressure threshold, a clear new phase can be observed. Furthermore, the new structure has also been analyzed by examining the radial distribution function and the detail atomic configurations, and the analysis shows a ABAB stacking sequence of the close-packed planes. Therefore, all of the evidences have shown the $\alpha\rightarrow\varepsilon$ phase transformation in iron under shock compression in our MD simulations.

A. Microview of phase transformation of iron with nanovoid under shock wave compression

Figure 1 shows the snapshots of the atoms in the nucleated area from the initial bcc structure to the final hcp structure from the MD simulations (piston velocity u_p =500 m/s). The traces of the atoms illustrate clearly dynamic procedure of the phase transformation in iron under shock loading. The course of the phase transformation contains two steps: first, the atoms in the (011) and (01−1) planes are compressed along the [100] direction to form a hexagon, and second, shuffles of alternate (011) and (01−1) planes in the [01−1] and [011] directions, respectively, create the hcp structure. By calculating the distance between the atoms, the evolution of the lattice parameters along with the phase transformation can be obtained. The distance of the atoms along the [100] direction and the [01−1] direction in the above case is shown in the Fig. 2, respectively. When the shock wave sweeps over the atoms,

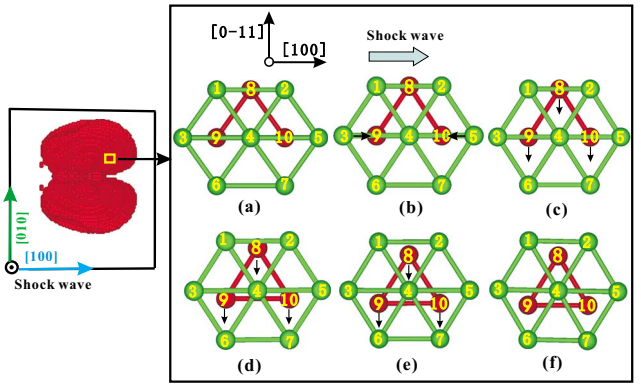

FIG. 1. (Color online) The traces of the atoms which come from the MD simulations show the dynamic phase transformation course from the bcc to hcp structure. The piston velocity is 500 m/s. The times for the snapshots are (a) 1.5 ps, (b) 1.9 ps, (c) 2.3 ps, (d) 3.2 ps, (e) 3.4 ps, and (f) 4.0 ps. The phase transformation mechanism suggests a two-step process, which contains a compression along the [100] direction and a shuffle along the [01−1] direction in the (011) plane. Pictures from (a) to (c) show that the compression of the lattice along the [100] direction, and pictures from (d) to (e) show the shuffle course along the [0−11] direction.

the distance between atoms 3 and 5 begins to decrease, and then the bcc lattice contracts along the [100] direction at about 10% and after 0.4 ps the contraction stops and the distance becomes stabilized. Meanwhile, the distance between atoms 2 and 7 has not changed, which means that the lattice does not elongate along the [01−1] direction even during the shuffle procedure. So far, the phase transformation finished its first step: the bcc (011) planes become the hcp (0002) planes. After that, as shown in Fig. 1, the atoms 8, 9, and 10 slip toward the [01−1] direction; that finally results

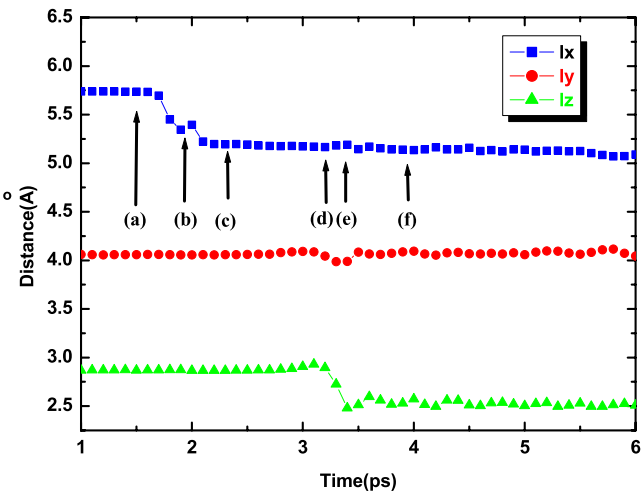

FIG. 2. (Color online) The distances of the atoms show the contraction procedure and the shuffle procedure under shock loading, respectively. *lx* shows the distance between atoms 3 and 5 in Fig. 1; *ly* shows the distance between atoms 2 and 7; *lz* shows the distance between atoms 4 and 8. The evolution of the distances of *lx* and *ly* show the compression along the [100] direction and no elongation along the [01−1] direction, and *lz* shows the shuffle procedure.

in the structure of hcp phase. The evolution of the distance between atoms 4 and 8 clearly shows the shuffle procedure (Fig. 2). Several regions have been checked to show the generality of this mechanism. The little plateau region in the compression procedure is only found in the region nearby the void (Fig. 2) because of relaxation effect of the rarefaction wave reflected from the surface of the void. The plateau becomes shorter where the region is farther away from the void. Except the effect of rarefaction wave, the above observation is in good agreement with the Hawreliak and coworkers'[22,23] results about the phase transformation mechanism. Although the bcc-hcp transformation occurs via the Nishiyama-Wassermann mechanism: $\{011\}_{bcc}\|\{0001\}_{hcp}$, it is worthy to point out by the MD simulation that among the three {011} family planes in the bcc structure, only the planes in parallel with the shock wave loading direction are slipped. The (011) and (01−1) planes are compressed to hexagonal pattern while other four {011} family planes are less strained because the shock loading lays in the (011) and (01−1) planes and the shock wave provides biggest compression along the [100] direction. Therefore the (011) and (01−1) planes are always compressed to be hexagonal pattern first. Thereafter, they take the second step to transform into hcp structure, leaving no chance to other family planes. The void does not change this geometrical effect. In the view of microstructure, the defective iron takes the same mechanism as that in the perfect iron.

B. Effect of the nanovoid

By comparing the response of the perfect single-crystal iron and the defective iron containing a nanovoid under shock loading, the effect of the nanovoid on the critical stress of phase transformation, the nucleation sites, the characteristic of phase-transition zone, and particle velocity profiles have been analyzed. When the shock stress is close to the threshold pressure, the influence of nanovoid to the phase transformation has been clearly observed. As the loading amplitude increases, the effect of nanovoid is overwhelmed by strong shock driving.

As the shock pressure reaches to certain threshold, the rearrangement of the atoms from bcc structure to hcp structure lowers the enthalpy of iron. The shuffling direction is perpendicular to the shock direction so as to adapt the path with the minimum-energy barrier. Meanwhile, this shuffling direction is perpendicular to the free surface of the void as well. The free surface gives the shuffling process more space than in perfect crystal, where the space is randomly generated by thermal fluctuation, and makes the embryo of hcp structure occur nearby the void surface much easier than inside of the perfect crystal. When the piston velocity is 350 m/s, (slower than the critical velocity 362 m/s for the phase transformation, corresponding to the shock pressure of 15 GPa), no nucleation site is observed in the perfect single-crystal iron. The corresponding pressure 14.5 GPa is not strong enough for the atoms to rearrange to form a new structure in the perfect crystal. However, the nucleation sites around the surface of the void are observed in the defective iron at the same piston velocity, and the abundance of the

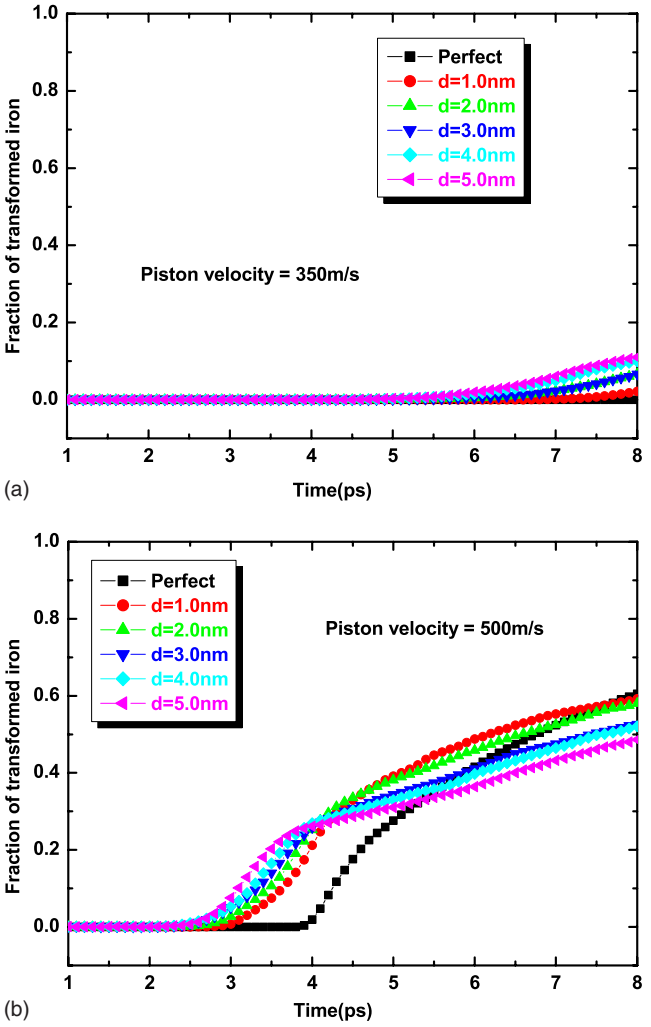

FIG. 3. (Color online) The comparison of the fraction of transformed material in the two kinds of samples: (a) Piston velocity is 350 m/s. (b) Piston velocity is 500 m/s. The influence of the void on the phase transformation velocity and quality can be found. The effects of the void size are also shown and the diameters are 1.0, 2.0, 3.0, 4.0, and 5.0 nm, respectively.

hcp structure atoms can reach 10% [Fig. 3(a)]. More clear influence of the nanovoid is observed at a stronger loading condition, where the piston velocity is 500 m/s (corresponding to a shock pressure of 21 GPa). At this loading condition, the nucleation sites are observed in both samples, but the nucleation sites appear later in the perfect single-crystal iron. For the defective iron, after 3.0 ps of simulation, the nucleation sites begin to appear and hcp phase expands outward from the edge of the nanovoid. However, in the perfect single-crystal iron, the nucleation sites do not appear until 4.0 ps [Fig. 3(b)]. Considering the voids with different volume, the phase transformation processes are complicated. The evolution of the fraction of hcp atoms for different size of void is illustrated in Fig. 3. Under the same loading strength, the atoms of hcp structures first appear in the sample which contains the biggest void. The bigger void size has faster nucleation speed. However, there is a turn point, after about 4.0 ps; the trends contradict that before [Fig. 3(b)]. Because before that time, the hcp region expands

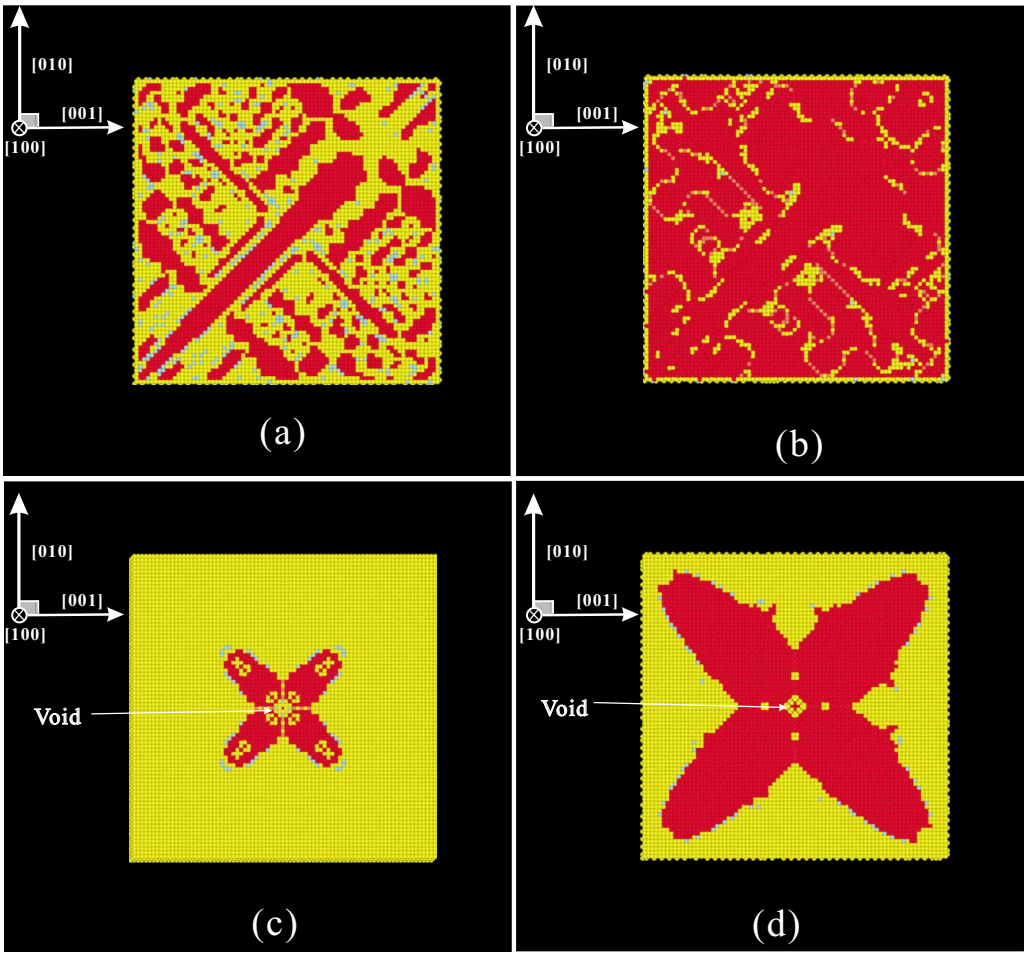

FIG. 4. (Color online) The cross section of the nucleation sites from the MD simulations (with u_p=500 m/s), showing nucleation sites growth under shock loading. The pictures (a) and (b) are obtained from the perfect single-crystal iron, (c) and (d) from the defective iron. The times for the snapshots are (a) 4.2 ps, (b) 4.6 ps, (c) 3.6 ps, and (d) 4.4 ps. The red shows the atoms with hcp structure, and the yellow shows the atoms with bcc structure; the other colors show the amorphous structure.

transversely and longitudinally, transverse expansion speed depends on the void size, and longitudinal expansion speed depends on the shock strength. After that time, hcp region reaches the transverse boundaries; the transformation speed only depends on the shock front. The bigger void attenuates more strength of the shock front and reduces the possibility for the nucleation after the shock front. Meanwhile, the bigger void reflects bigger rarefaction wave, which reverse much more hcp structures back to bcc structure. For perfect crystal, the nucleation sites are randomly distributed behind the shock front, and then those nucleation sites expand and connect to form a plane boundary, which is similar to that observed by Kadau *et al.*[12,13] The transformation front is created on a picosecond time scale. With the time going, the nucleation sites expand and touch each other, and the large scale phase transformation zones are observed [Figs. 4(a) and 4(b)]. In the defective iron, the hcp structure initiates from four symmetric locations on the surface of the void and expands outward to form a "butterfly" phase-transition zone [Figs. 4(c) and 4(d)]. With the shock front propagating, the butterfly shape grows up gradually. When the shock pressure increases further, the nucleation nearby the nanovoid is overwhelmed by the random nucleation and the effect of nanovoid becomes diminished.

The effect of the nanovoid on the phase transformation is also shown from the particle velocity profiles. Slightly above the transformation threshold, shock waves in the [100] direction exhibit the split two wave structures, as shown in Fig. 5, where the particle velocity is 500 m/s, and the elastic precursor is followed by the transformation wave. At the time of shocked for 3.0 ps, when the shock wave just sweeps over the nanovoid in the defective iron, there are no difference from the particle velocity profiles in the two kind of samples [Fig. 5(a)]. However, when the shock wave sweeps over the nanovoid for a moment, nucleation sites have grown up, and the effect of the nanovoid on the particle velocity profile can be observed obviously, such as shocked for 5.0 ps. It is shown that the particle velocity from the defective iron is lower than that from the perfect single-crystal iron [Fig. 5(b)]. The effect of the void size in the particle velocity profiles is also shown in Fig. 5. The larger void has lower particle velocity profile. When the shock wave sweeps over the nanovoid, there are excited regions around the edge of the nanovoid, which are referred to as hot spot.[24] The tem-

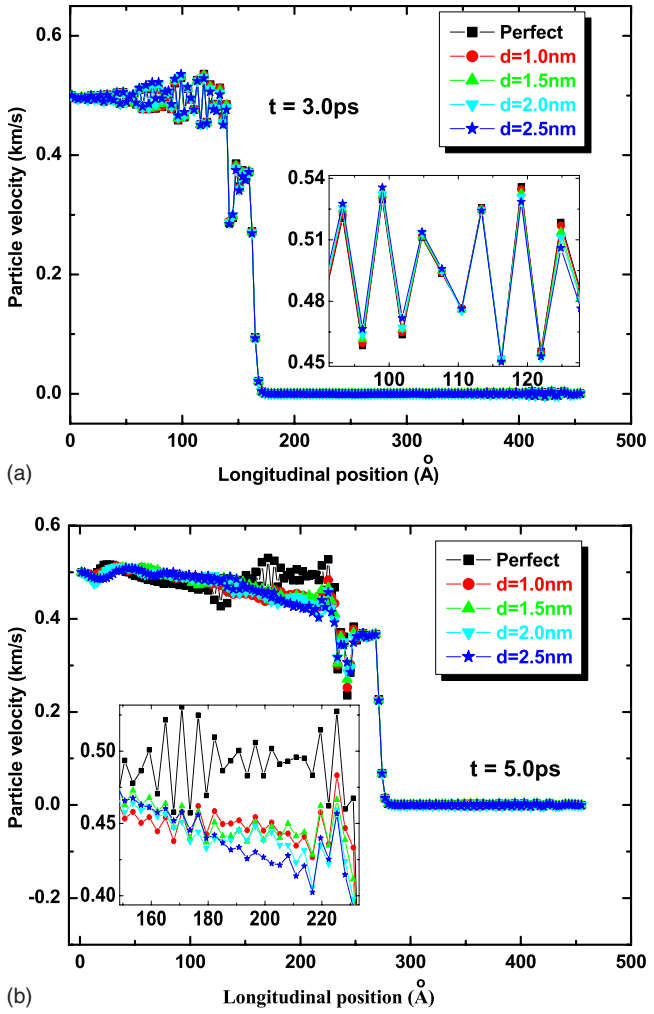

FIG. 5. (Color online) Particle velocity profiles for shocks along the [100] direction as obtained from the MD simulations (u_p =500 m/s): (a) 3.0 ps, (b) 5.0 ps. From the particle velocity profile, the effects of the void size can also be shown. The existence of the void induces hot spot and changes the macroscopic response, such as lower particle velocity in the defective iron than in the perfect iron.

perature of hot spot inside the nanovoid is enhanced during the compression because of the focusing of the momentum and energy toward the void.[25] Figure 6 depicts representation of the effective kinetic temperature when the shock wave just passes through the void, the T_k is defined what the $3K_BT_K/2$ equals the kinetic energy per particle. The partial shock energy relaxes into the thermal energy through the void collapse, which induces the lower particle velocity in the defective iron.

C. Effect of the shear stress

The shear stress drives the atoms in the (011) and (01 −1) planes to move to create the hcp structure. Under the uniaxial strain conditions, a large shear stress would be produced in the shock compressed material due to the strong lateral confinement. The relaxation of energy makes the shear stress to drive the atoms to slip to rebuild a new structure. The shear stress perpendicular to the shock loading appears to make the atoms in the (011) and (01−1) planes slip along the [01−1] and [011] directions. When the shock wave is along ⟨110⟩ or ⟨111⟩ directions, the situations will be different, and the resolved shear stress is not zero by resolving the primary stress.

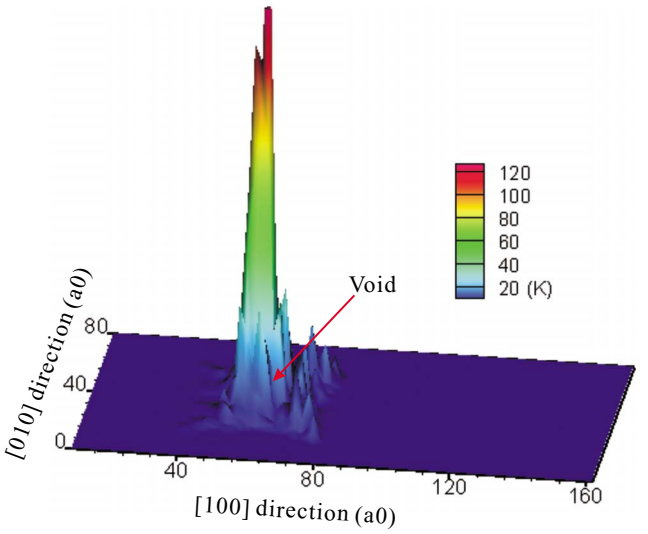

FIG. 6. (Color online) Color depiction representation of local effective kinetic temperature in the vicinity of the void defect for 500 m/s piston velocity simulation at a time of 3.0 ps. The color scale corresponds to the temperature, and the a0 is the lattice constant.

The distribution of the resolved shear stress has been computed to show the relationship of the slip planes and the shear stress. As shown in Fig. 7, the resolved shear stress along slip planes has been depicted, where the piston velocity is 500 m/s, and the atoms in the figures are colored according to the intensity of the shear stress. Figure 7(a) shows the (100) plane cut from the defective iron. The yellow atoms illustrate the position of the maximum shear stress, the red atoms take the second any maximum, and the blue atoms are where the shear stress is close to zero. Figure 7(b) is the (100) cross section of the phase transformation nucleation site. It is found that nucleation sites are consistent with the distribution of the shear stress. The red salience shows that the maximum resolved shear stress is in the (011) and (01 −1) planes around the edge of the void, which are just the slip planes of the phase transformation. The three-dimensional (3D) snapshot of the shear stress from the MD simulations is shown in Fig. 7(c), and the maximum shear stress is only shown, while other area where the shear stress is smaller has been expunged for clarity. The atoms whose shear stress is largest slip first along the slip plane. It is noticeable that the area of the maximum shear stress is consistent with the phase transformation nucleation [Fig. 7(d)]. The position of the maximum resolved shear stress is accurately in the (011) and (01−1) planes which are parallel with the shock loading direction. The zone of the maximum resolved shear stress along the slip plane is just a butterfly shaped pattern, which is consistent with the phase transformation nucleation sites.

The comparison of the shock response from the two kinds of the samples is shown in Fig. 8, where the piston velocity

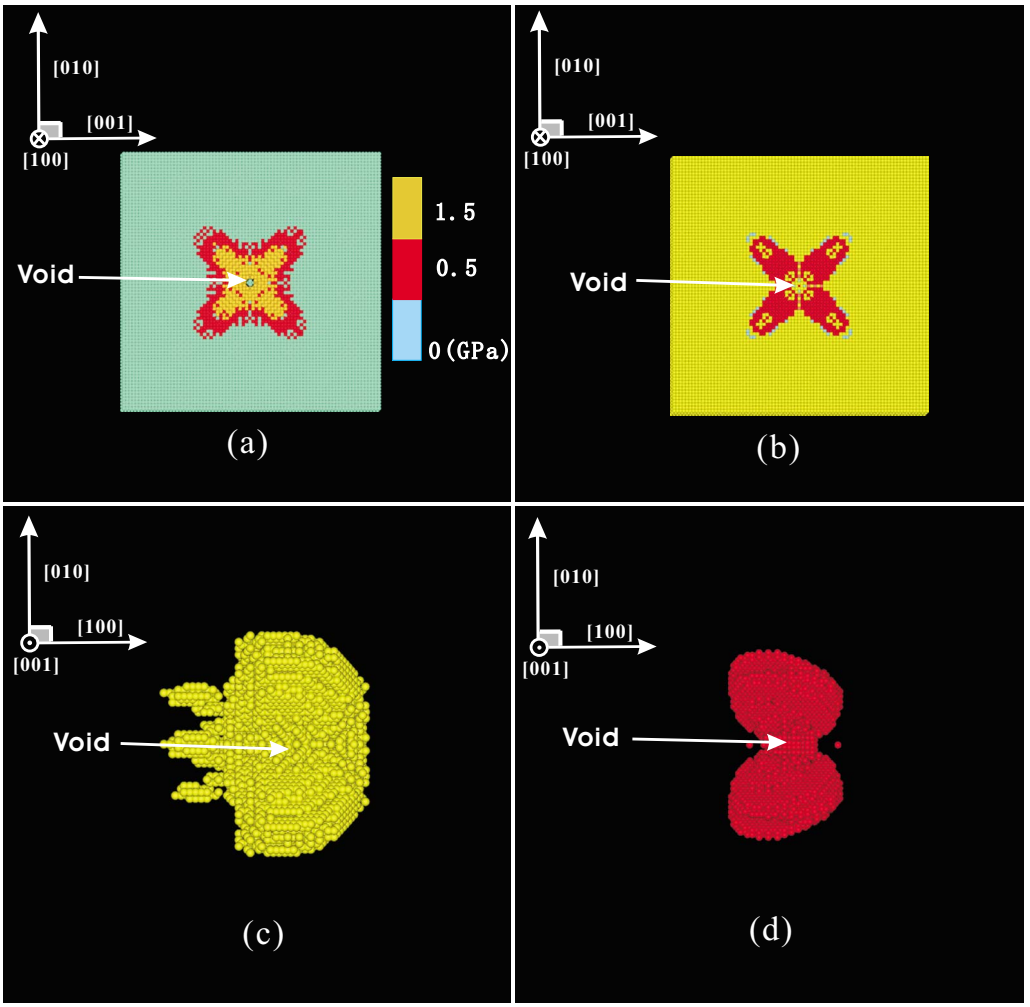

FIG. 7. (Color online) (a) The (100) plane cut from the defective iron, the color is according to the intensity of the resolve shear stress. (b) The nucleation sites section from the MD simulation. Only the atoms with hcp structure are shown; other atoms are deleted for clarity. (c). The 3D snapshot of the maximum resolve shear stress, and only the maximum resolve shear stress is shown, the others are expunged. (d). The 3D snapshot of the nucleation sites, which is in agreement with the shape of the nucleation sites.

is 500 m/s. The evolution of the shear stress in the (011) planes has been shown, and the two family pictures are cut from the same position in the two samples. The above four pictures are cut from the perfect single-crystal iron, and the neither four pictures are from the defective iron. So we can compare the evolution of the shear stress in the two samples under the same shock loading, which can help us understand different nucleation sites under shock loading. In the perfect single-crystal iron, it is found that the shear stress expands with the time going from the above pictures gradually (Fig. 8). The shear stress first concentrates behind the shock wave front, where the maximum shear stress first appears. In the effect of the shear stress, the atoms begin to slip along the slip plane, therefore the embryo of hcp structure is randomly activated behind the shock front in the perfect single crystal. However it is very different in the defective iron; the nucleation sites first occur near the edge of the void. When the shock wave sweeps over the void, the free surface gives the shuffling process more space than in perfect crystal, and the shear stress around edge of the void is easier concentrated. The maximum resolve shear stress first appears around the

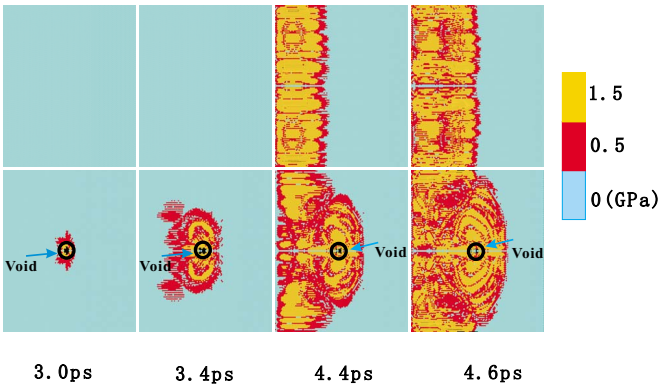

FIG. 8. (Color online) The comparison of the (011) plane in the two samples according to the distribution of the resolve shear stress: the above four pictures are cut from the perfect single-crystal iron; the other four pictures are cut from the defective iron. The figures show the change of the shear stress in iron under shock loading. The circle shows the position of the void.

edge of the void, and the embryo of hcp structure occurs nearby the void surface. All the evidences have shown that the shear stress affects the phase transformation, and the important role of the shear stress on the phase transformation is outlined.

IV. CONCLUSION

The interaction of the shock wave with a pre-existing nanovoid and the role of the shear stress in the course of the phase transformation of iron have been studied. The results show that the nanovoid is the favorite nucleation site of the phase transformation of iron and it accelerates the phase-transition zone growth. The existence of the nanovoid also decreases the pressure threshold of the phase transformation, and makes the nucleation sites present a butterfly-shaped pattern. Meanwhile, the existence of the nanovoid induces hot spot and changes the macroscopic response, such as lower particle velocity in the defective iron. The void size also affects the threshold pressure and the nucleation speed, and the influence of the void size is also shown from the particle velocity profiles. By calculating the distribution of the resolve shear stress along the slip plane, the important role of the shear stress on the phase transformation is also outlined. At the same time, the relationship between the shear stress and the slip planes has been discussed. The results indicate that the defects play an important role in shock-induced phase transformation.

ACKNOWLEDGMENTS

This research was supported by NASF Project No. 10476027 of the National Nature Science of China, and by Grant No. 2007A01004 from the Science and Technology Foundation of China Academy of Engineering Physics, and as well by Grant No. 2002cb412701 from the 973 Threshold Project of China. The authors would like to thank Xingqian Zhang and Fuqian Jing for helpful discussions.

*Author to whom all correspondences should be addressed: honglianghe@263.net

[1] F. Birch, J. Geophys. Res. **57**, 227 (1952).
[2] O. L. Anderson, Nature (London) **314**, 407 (1985).
[3] L. M. Barker and R. E. Hollenbach, J. Appl. Phys. **45**, 4872 (1974).
[4] D. Bancroft, E. L. Peterson, and S. Minshall, J. Appl. Phys. **27**, 291 (1956).
[5] H. K. Mao, W. A. Bassett, and T. Takahashi, J. Appl. Phys. **38**, 272 (1967).
[6] P. M. Giles, M. H. Longenbach, and A. R. Marder, J. Appl. Phys. **42**, 4290 (1971).
[7] B. Yaakobi, T. R. Boehly, D. D. Meyerhofer, T. J. B. Collins, B. A. Remington, P. G. Allen, S. M. Pollaine, H. E. Lorenzana, and J. H. Eggert, Phys. Rev. Lett. **95**, 075501 (2005).
[8] W. A. Bassett and E. Huang, Science **238**, 780 (1987).
[9] F. M. Wang, R. Ingalls, and E. D. Crozier, Jpn. J. Appl. Phys., Suppl. **32-2**, 749 (1993).
[10] F. M. Wang and R. Ingalls, Phys. Rev. B **57**, 5647 (1998).
[11] K. Kadau, T. C. Germann, P. S. Lomdahl, and B. L. Holian, Science **296**, 1681 (2002).
[12] K. Kadau, T. C. Germann, P. S. Lomdah, and B. L. Holian, Phys. Rev. B **72**, 064120 (2005).
[13] K. Kadau, T. C. Germann, P. S. Lomdahl, and B. L. Holian, Phys. Rev. Lett. **98**, 135701 (2007).
[14] K. J. Caspersen, A. Lew, M. Ortiz, and E. A. Carter, Phys. Rev. Lett. **93**, 115501 (2004).
[15] U. Pinsook and G. J. Ackland, Phys. Rev. B **62**, 5427 (2000).
[16] W. J. Zhu, Z. F. Song, X. L. Deng, H. L. He, and X. Y. Cheng, Phys. Rev. B **75**, 024104 (2007).
[17] M. S. Daw and M. I. Baskes, Phys. Rev. Lett. **50**, 1285 (1983).
[18] M. I. Baskes, Phys. Rev. B **46**, 2727 (1992).
[19] R. Harrison, A. F. Voter, and S. P. Chen, in *Atomistic Simulation of Materials*, edited by V. Vitek and D. J. Srolovitz (Plenum, New York, 1989), p. 219.
[20] B. L. Holian and P. S. Lomdahl, Science **280**, 2085 (1998).
[21] J. D. Honeycutt and H. C. Andersen, J. Phys. Chem. **91**, 4950 (1987).
[22] J. Hawreliak, J. D. Colvin, J. H. Kalantar, H. E. Lorenzana, J. S. StÖlken, H. M. Davies, T. C. Germann, B. L. Holian, K. Kadau, P. S. Lomdahl, A. Higginbotham, K. Rosolankova, J. Sheppard, and J. S. Wark, Phys. Rev. B **74**, 184107 (2006).
[23] D. H. Kalantar, J. F. Bleak, G. W. Collins, J. D. Colvin, H. M. Davies, J. H. Eggert, T. C. Germann, J. Hawreliak, B. L. Holian, K. Kadau, P. S. Lomdahl, H. E. Lorenzana, M. A. Meyers, K. Rosolankova, M. S. Schneider, J. Sheppard, J. S. StÖlken, and J. S. Wark, Phys. Rev. Lett. **95**, 075502 (2005).
[24] J. P. Dear, J. E. Field, and A. J. Walton, Nature (London) **332**, 505 (1988).
[25] T. Hatano, Phys. Rev. Lett. **92**, 015503 (2004).